DYNAMIC CHARACTERISTICS OF V-SHAPED POCKET BEARING UNDER THERMAL-MECHANICAL COUPLING EFFECT

Jie HUANG [1], Yanbin LIU [1,2,*], Xuying LI[1], Kun YANG[1], Jinbo LING[1]

Aiming at the problem of thermal deformation in bearing at high rotation speed, which affects the working accuracy of bearing, the influence of thermal-mechanical coupling on the dynamic characteristics of V-shaped pocket cylindrical roller bearing was studied. The heat transfer theory was used to establish the bearing thermal network model considering the V-shaped pocket, and the temperature of each node and the thermal deformation of each component were obtained. The bearing dynamics model considering thermal-mechanical coupling was established by combining with multi-body dynamics theory. The effect of the operating conditions on the thermal deformation of the V-shaped pocket was analyzed, and the evolution law of cage slip rate and the collision force between the roller and V-shaped pocket under the action of thermal-mechanical coupling was explored. The results indicate that under high rotation speed and light load, the influence of speed and load on the temperature rise and thermal deformation of the V-shaped pocket is relatively small. However, when the rotation speed is in the range of 18000~21000r/min, the cage slip rate decreases with the increase of speed, while when the load is in the range of 100~500N, the cage slip rate increases with the growth of load. In addition, the collision force between the roller and V-shaped pocket under the consideration of thermal deformation increases greatly compared with that without thermal deformation.

Keywords: Cylindrical roller bearing; V-shaped pocket; Thermal network model; Thermal-mechanical coupling; Dynamics model; Dynamic characteristics

1. Introduction

The aero-engine main shaft bearing is subject to thermal deformation of components due to frictional heat generation, significantly affecting the bearing dynamic characteristics[1]. Meanwhile, the thermal-mechanical coupling mechanism of the bearing and its dynamic characteristics under the action is very complex[2]. Therefore, it is of great practical significance to study the dynamic characteristics of the bearing under the action of thermal-mechanical coupling. Yan et al.[3] proposed a thermal network model for the spindle bearing considering thermal-structural coupling and obtained the bearing temperature rise curve and characteristics and the influence of temperature on bearing structural deformation.

[1] School of Mechatronics Engineering, Henan University of Science and Technology, Luoyang Henan 471003, China
[2] Collaborative Innovation Center of Machinery Equipment Advanced Manufacturing of Henan Province, Henan University of Science and Technology, Luoyang Henan 471003, China
* Corresponding author: liuyb2018@haust.edu.cn

Yu et al.[4] established the steady-state thermal network model to analyze the thermal deformation of bearing components caused by temperature rise at each bearing node under different operating conditions, the coupling relationship between the thermal and dynamic characteristics of the bearing obtained. Cao et al.[5] established a bearing heat balance model using the thermal network method based on the bearing thermal-mechanical and dynamics theory, and analyzed the bearing dynamic characteristics under the thermal-mechanical coupling effect. Gao et al.[6] developed an improved bearing multi-node thermal network method based on Hertz thermal diffusion theory to get more accurate internal node temperatures of the bearing. Zhang et al.[7] obtained the temperature of each node in the thermal network based on the bearing local heat generation model and the multi-node thermal network method and analyzed the effect of thermal deformation on the bearing characteristics.

The research of the above scholars mostly focuses on the common bearing temperature rise and thermal deformation, but less attention is paid to the bearing dynamic characteristics under the effect of thermal-mechanical coupling. The V-shaped pocket cylindrical roller bearing has good stability and anti-slip performance[8], but the influence mechanism of the V-shaped pocket cage on the bearing heat transfer is still unclear, and the effect of its thermal-mechanical coupling on the bearing dynamic characteristics is also not clear.

In this paper, the thermal network method was used to establish the heat transfer model considering the structure of the V-shaped pocket, and the bearing dynamic model was established under the action of thermal-mechanical coupling to explore the influence on the bearing dynamic characteristics and provide the theoretical basis for studying the dynamic characteristics of the V-shaped pocket cylindrical roller bearing.

2. Dynamic model of the V-shaped pocket bearing

2.1. Thermal deformation for bearing components

Due to the frictional heat generation between the bearing components, the increase in bearing temperature will lead to thermal deformation of the components and affect the bearing dynamic characteristics. Therefore, the equation given by Harris[9] was used to calculate the thermal deformation of the V-shaped pocket cylindrical roller bearing components.

$$u_i^k = \Gamma_i \Delta T_i d_i;\ u_o^k = \Gamma_o \Delta T_o d_o;\ u_r^k = \Gamma_r \Delta T_r d_r \tag{1}$$

Where u^k is the thermal deformation of bearing components; Γ is the coefficient of thermal deformation; ΔT is the temperature rise; d is the diameter of each bearing component; Subscripts i, o and r represent the inner ring, outer ring and roller respectively.

Then the diameter of each component after thermal deformation is

$$\tilde{d}_i^k = d_i + u_i^k;\ \tilde{d}_o^k = d_o + u_o^k;\ \tilde{d}_r^k = d_r + u_r^k \tag{2}$$

Due to the special structure of the V-shaped pocket wall, it is approximated as a rigid plane to simplify the calculation, as shown in Fig. 1.

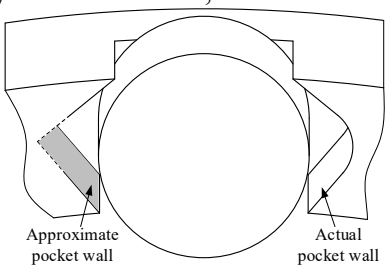

Fig.1. Diagram of V-shaped Pocket

The thermal deformation of the pocket wall can be expressed as[10]

$$u_p^k = \frac{1}{E}\left[\frac{Afx + Bfy}{y^2} - \frac{\mathrm{v}(Cfx + Dfy)}{x^2}\right] \tag{3}$$

Where E is the elastic modulus; A、B、C、D is polynomial fitting constant; x、y is the length and width of the pocket wall, respectively; v is Poisson's ratio; $f = F(E, \Delta T, k, V)$, determined by the material's properties, shape factor, and temperature rise[10].

The clearance between the pockets under the action of thermal deformation is

$$\tilde{\sigma}^k = \sigma - u_r^k - u_p^k \tag{4}$$

Where σ is the initial pocket clearance.

2.2. Model of V-shaped pocket and roller interaction

The interaction model of the roller and the V-shaped pocket cylindrical roller bearing is shown in Fig. 2. Where α is the inclination angle of the pocket a and c walls; β is the inclination angle of the pocket b and d walls; $\{O, x, y\}$ is the geometric center coordinate system of the pocket. $\{O, x_i, y_i\}$ is the ideal coordinate system of the roller, which is determined by the actual position of the roller in motion. $\{O_j, x_j, y_j\}$ is the roller centroid coordinate system.

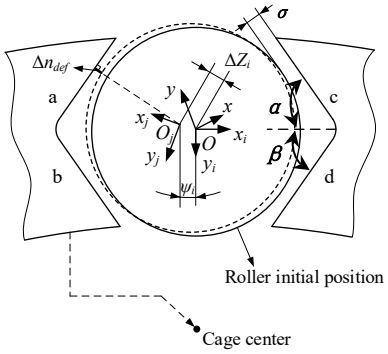

Fig.2. Model of interaction between roller and pocket

The minimum clearance between the roller and the pocket wall is

$$\Delta n_{def} = \Delta Z_i - \tilde{\sigma}^k \tag{5}$$

Where n is the pocket wall (n=a, b, c, d); $\tilde{\sigma}^k$ is the pocket clearance under thermal-mechanical coupling; ΔZ_i is the absolute value of the circumferential component of the roller mass center in the ideal coordinate system, which can be expressed as

$$\Delta Z_a = \Delta Z_c = x_{ri} \cdot \cos\psi_i \cdot \sin\alpha$$
$$\Delta Z_b = \Delta Z_d = x_{ri} \cdot \cos\psi_i \cdot \sin\beta$$

Where x_{ri} is the moving component of the roller mass center in the direction of x_i in the ideal coordinate system; ψ_i is the angular displacement of the roller mass center.

When the minimum oil film thickness $\Delta_{cl} \geq \Delta n_{def} \geq 0$, the contact between the roller and the pocket wall is affected by Hertz line contact and hydrodynamic pressure.

Considering the actual lubrication state between the roller and the pocket, as shown in Fig. 3, the roller-to-pocket contact zone is divided into the lubricating oil inlet zone, the Hertz contact zone, and the lubricating oil outlet zone.

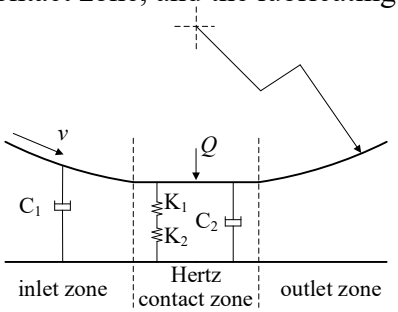

Fig.3. Stiffness and damping of the contact zone between the roller and the pocket wall

Since the contact stiffness in the inlet zone is much smaller than that of the Hertz contact zone, it is ignored[11]. Therefore, the contact stiffness between the roller and the pocket is mainly composed of the Hertz contact stiffness and the oil film stiffness in series within the Hertz contact zone, which can be expressed as

$$K = \frac{K_1 K_2}{K_1 + K_2} \tag{6}$$

According to Hertz line contact theory, the contact stiffness between the roller and the pocket in the Hertz contact zone is[12]

$$K_1 = 2.89 \times 10^7 l^{0.8} Q^{0.1} \tag{7}$$

Where l is the roller length; Q is the normal load.

The oil film stiffness between the roller and pocket in the contact zone is[13]

$$K_2 = \frac{-459 E^{0.03} Q^{1.1}}{a^{0.54} (\eta v_i)^{0.7} R^{0.43} l^{0.13}} \tag{8}$$

Where a is the viscosity pressure coefficient of lubricating oil; η is the lubricating oil viscosity; R is the equivalent radius of the contact zone.

The damping of the contact zone between the roller and the pocket is

$$C = C_1 + C_2 \tag{9}$$

Where C_2 is the structural damping of the Hertz contact zone; The inlet zone damping C_1 can be expressed as[14]

$$C_1 = \frac{2.12\pi\eta r^{1.5} L_M}{\Delta_{cl}^{1.5}} \tag{10}$$

Where r is the roller radius; L_M is the contact half-width.

According to the method proposed by Dowson-Higginson for calculating the oil film thickness of the elastohydrodynamic lubrication in the state of line contact, The minimum oil film thickness in the Hertz contact zone can be determined as[15]

$$\Delta_{cl} = 1.17R(aE)^{0.57}(\frac{\eta v_i}{ER'})^{0.69}(\frac{Q}{ER'})^{-0.13} \tag{11}$$

Where R' is the equivalent curvature radius of two contact bodies.

The normal contact force between the roller and pocket wall is[16]

$$F_{nri} = K_{cl}\delta_{nri}^{10/9} + C_{cl}\delta_{nri}^{10/9}\dot{\delta}_{nri} + \frac{2.44\eta|v_i + v_{pi}|rl}{\Delta_{cl}} \tag{12}$$

Where δ_{nri} is the roller offset value, $\delta_{nri} = \Delta_{cl} - \Delta n_{def}$; v_i and v_{pi} are the tangential speed of the roller and pocket wall, respectively.

The friction force between the roller and the pocket wall is

$$T_{nri} = \mu_n F_{nri} \tag{13}$$

Where μ_n is the friction coefficient between the roller and cage pocket, according to the sliding friction relationship between the roller and the pocket wall[8], μ_n is taken as 0.1.

When the minimum clearance $\Delta n_{def} \geq \Delta_{cl}$, under the action of hydrodynamic pressure, the normal contact force between the roller and pocket wall is[17]

$$F_{nri} = \frac{2.44\eta|v_i + v_{pi}|rl}{\Delta_{cl}} \tag{14}$$

The friction force between the roller and the pocket wall is[8]

$$T_{nri} = \frac{1.16\Delta_{cl}F_{nri}|v_i - v_{pi}|}{|v_i + v_{pi}|\Delta n_{def} r^{1/2}} \tag{15}$$

To save paper space, the interaction models between the roller and ring raceway, cage and ring guide surface can be found in the Reference[18] and will not be discussed in this paper.

3. Model of thermal network for the V-shaped pocket bearing

Based on the frictional heat generation analysis model of V-shaped pocket cylindrical roller bearing[18], the frictional heat generation between the components is obtained. The heat conduction and convection inside the bearing are studied according to the heat transfer theory[19].

The thermal network model constructed for bearing heat transfer is mostly based on five-node and seven-node models[20]. Moreover, the bearing mostly adopts the conventional cage, and there is a lack of consideration of the influence of the special pocket structure cage on the heat transfer. Therefore, a bearing multi-node thermal network model is established based on the V-shaped pocket structure of the cage. The heat transfer inside the V-shaped pocket cylindrical roller bearing mainly includes the heat conduction between the roller and the inner and outer ring raceway, the inner ring and the main shaft, the outer ring and the housing, and the heat convection between the components and the lubricating oil. Furthermore, the heat conduction between the roller and each pocket wall, the pocket walls and the cage over-beam are considered[21], as shown in Fig. 4 (a), and the temperature nodes are provided in each unit structure of the bearing, as shown in Fig. 4 (b).

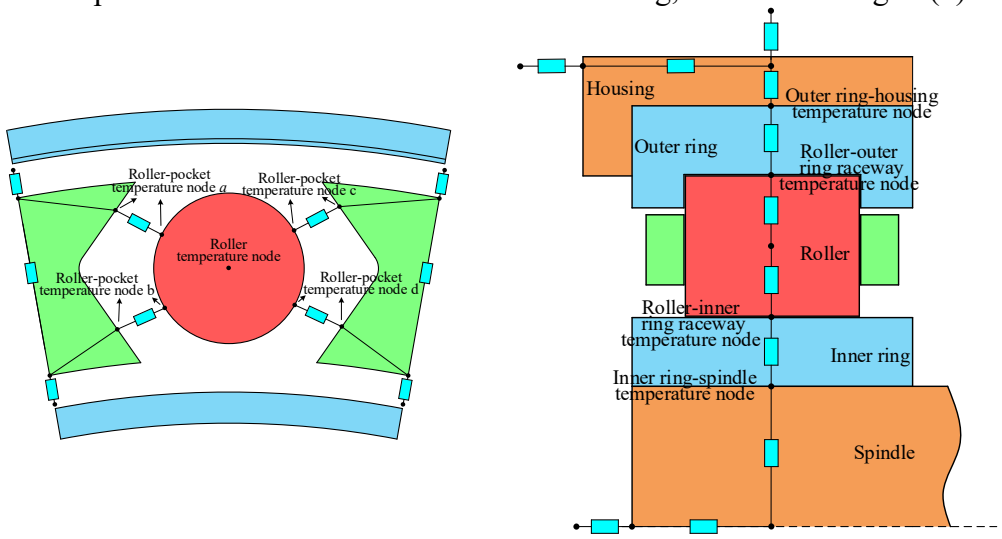

(a) Cage temperature nodes diagram (b) Bearing temperature nodes diagram

Fig.4. Temperature node diagram of bearing components

According to the energy balance principle and Kirchhoff's law, for each thermal node, the inflow heat E_{in} equals the outflow heat E_{out}, and each node is connected in thermal resistance to form a thermal network. Therefore, based on the temperature nodes of each unit structure of the bearing, the heat transfer network of the V-shaped pocket cylindrical roller bearing is shown in Fig. 5.

Where T_r, T_i and T_o are roller, inner and outer ring raceway temperature respectively; T_{oil} is the lubricating oil temperature; T_{air} is the room temperature; T_a, T_b, T_c and T_d are the wall temperatures of the cage pocket respectively. T_{h1}, T_{h2}, T_{h3} are the temperatures at each node of the bearing housing, respectively; T_{s1}, T_{s2}, T_{s3} are the temperatures at each node of the main shaft, respectively; R is the thermal resistance between the corresponding nodes, which the type of material, geometry, and heat transfer can determine[4].

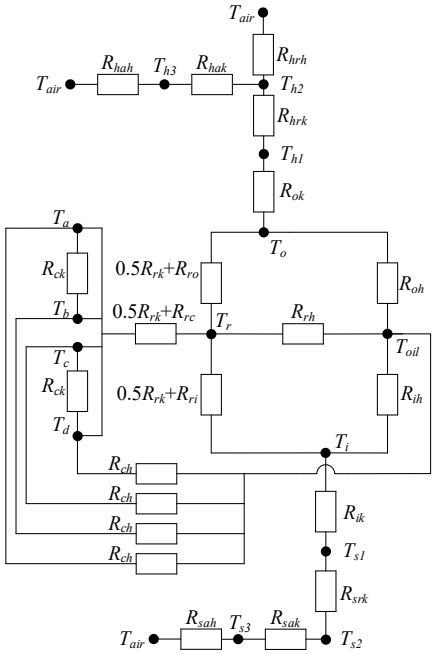

Fig.5. Diagram of heat transfer network

According to the analytical theory of Burton[22], the frictional heat generated by the bearing each heat source is distributed in a ratio of 1:1, and according to the bearing heat transfer network, the heat balance equations are established as shown in Eq. (16)~ (25), which are solved using the Gaussian Saidel iterative method, and the temperature of each node can be obtained.

$$\frac{T_r-T_i}{0.5R_{rk}+R_{ri}}+\frac{T_r-T_o}{0.5R_{rk}+R_{ro}}+\frac{T_r-T_{oil}}{R_{rh}}+\frac{4T_r-T_a-T_b-T_c-T_d}{2R_{rk}+4R_{rc}}=\frac{H_{ni}+H_{Ii}+H_{Oi}}{2}+H_{fi} \tag{16}$$

$$\frac{T_i-T_r}{0.5R_{rk}+R_{ri}}+\frac{T_i-T_{s1}}{R_{ik}+R_{ih}}+\frac{T_i-T_{oil}}{R_{ih}}=\frac{H_{Ii}}{2} \tag{17}$$

$$\frac{T_o-T_r}{0.5R_{rk}+R_{ro}}+\frac{T_o-T_{h1}}{R_{ok}+R_{oh}}+\frac{T_o-T_{oil}}{R_{oh}}=\frac{H_{Oi}+H_g}{2} \tag{18}$$

$$\frac{T_a-T_r}{0.5R_{rk}+R_{rc}}+\frac{T_a-T_b}{R_{ck}}+\frac{T_a-T_{oil}}{R_{ch}}=\frac{H_{ai}}{2} \tag{19}$$

$$\frac{T_c-T_r}{0.5R_{rk}+R_{rc}}+\frac{T_c-T_d}{R_{ck}}+\frac{T_c-T_{oil}}{R_{ch}}=\frac{H_{ci}}{2} \tag{20}$$

$$\frac{T_b-T_r}{0.5R_{rk}+R_{rc}}+\frac{T_b-T_a}{R_{ck}}+\frac{T_b-T_{oil}}{R_{ch}}=\frac{H_{bi}}{2} \tag{21}$$

$$\frac{T_d-T_r}{0.5R_{rk}+R_{rc}}+\frac{T_d-T_c}{R_{ck}}+\frac{T_d-T_{oil}}{R_{ch}}=\frac{H_{di}}{2} \tag{22}$$

$$\frac{T_{s1}-T_i}{R_{ik}}+\frac{T_{s1}-T_{s2}}{R_{srk}}=\frac{T_{s2}-T_{s1}}{R_{srk}}+\frac{T_{s2}-T_{s3}}{R_{sak}}=\frac{T_{s3}-T_{s2}}{R_{sak}}+\frac{T_{s3}-T_{air}}{R_{sah}} \tag{23}$$

$$\frac{T_{h2}-T_{h1}}{R_{hrk}}+\frac{T_{h2}-T_{h3}}{R_{hak}}+\frac{T_{h2}-T_{air}}{R_{hrh}}=0 \tag{24}$$

$$\frac{T_{h1}-T_{h2}}{R_{hrk}}+\frac{T_{h1}-T_o}{R_{ok}}=\frac{T_{h3}-T_{h2}}{R_{hak}}+\frac{T_{h3}-T_{air}}{R_{hah}} \tag{25}$$

Where H is the frictional power loss generated by each bearing heat source[18]. H_{Ii} and H_{Oi} are sliding frictional power loss of roller and ring raceway respectively; H_{ni} is the sliding frictional power loss between the roller and pocket wall (n=*a, b, c, d*); H_{fi} is the frictional power loss of roller oil churning; H_g is the sliding frictional power loss between cage and ring guide surface.

Under thermal-mechanical coupling, the dynamic characteristics analysis process of the V-shaped pocket cylindrical roller bearing is shown in Fig. 6.

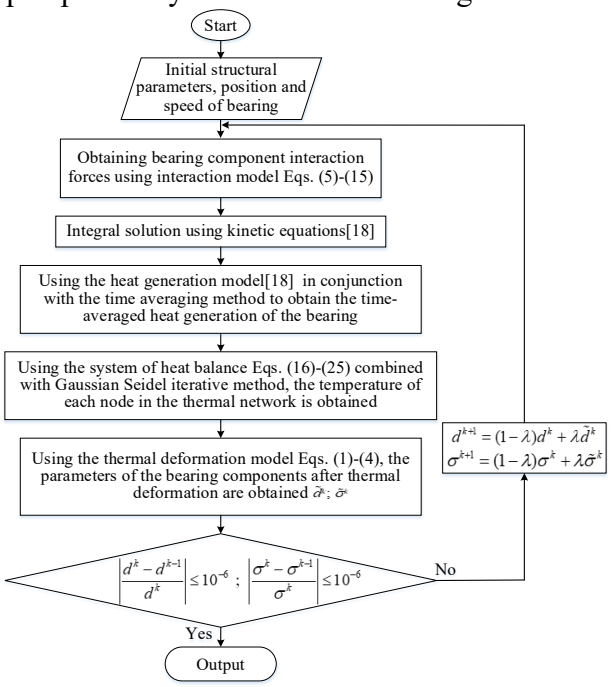

Fig.6. Model solving flowchart

4. Analysis model correctness verification

Based on the main geometric parameters of cylindrical roller bearing in Reference[23] were used to establish the dynamic model and multi-node thermal network model of the bearing by the above modeling method. The temperature rise of the bearing outer ring raceway under different operating conditions was simulated, and the simulation data and the experimental data in the reference were compared and analyzed to verify whether the model proposed in this paper is correct and reasonable. The comparison between simulation data and experimental data is shown in Fig. 7.

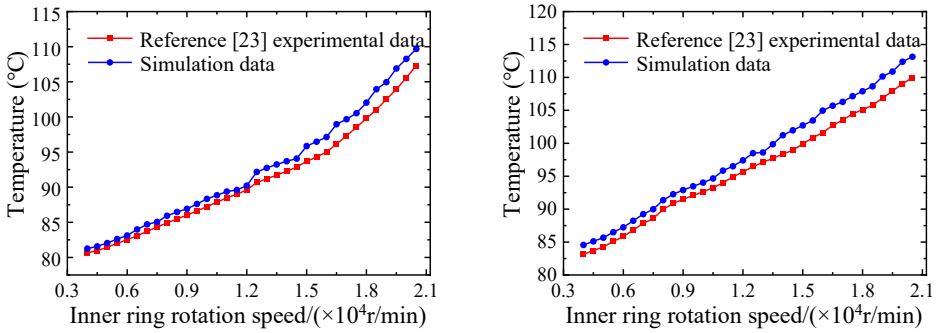

(a) radial load 111N (b) radial load 445N

Fig.7. Comparison between simulation and experimental data of outer ring raceway temperature

As shown in the figure, the temperature curve of simulation data has some unevenness, which is mainly caused by the non-uniformity of dynamic integration error. However, the temperature rise trend of the simulation data and the experimental data is basically consistent, and the maximum temperature error is 3%. Therefore, the dynamic model and thermal network model proposed in this paper have high reliability.

5. Effect of thermal-mechanical coupling on bearing dynamic characteristics

5.1. Bearing main parameters

Based on the influence law of V-shaped pocket geometry parameters on pocket frictional heat generation[18], the inclination angles α and β of the cage pocket wall are respectively 40 ° and 50 °. The main geometric parameters of the bearing are shown in Table 1. Aviation lubricating oil 4109 is selected for bearing lubrication, and its initial parameters are shown in Table 2.

Table 1

Geometric parameters of the bearing

Parameter	Numerical value	Parameter	Numerical value
Inner ring diameter (mm)	100	Roller diameter (mm)	10
Outer ring diameter (mm)	140	Roller length (mm)	7
Bearing width (mm)	20	Cage inner diameter (mm)	114.46
Number of rollers	26	Cage outer diameter (mm)	124.46

Table 2

Parameters of 4109 aviation lubricating oil

Parameter	Numerical value
Density (kg/mm^3)	8.6E-07
Viscosity (Pa·s)	3.3E-02
Heat conduction coefficient (N·s^{-1}·°C^{-1})	9.66E-02
Viscosity-pressure coefficient (Pa^{-1})	1.28E-08
Viscosity-temperature coefficient (°C^{-1})	3.2E-02

5.2. Analysis of thermal characteristics for V-shaped pocket bearing

In the case of room temperature 25℃, Fig. 8 shows the temperature variation trend of each component of the V-shaped pocket bearing under different operating conditions.

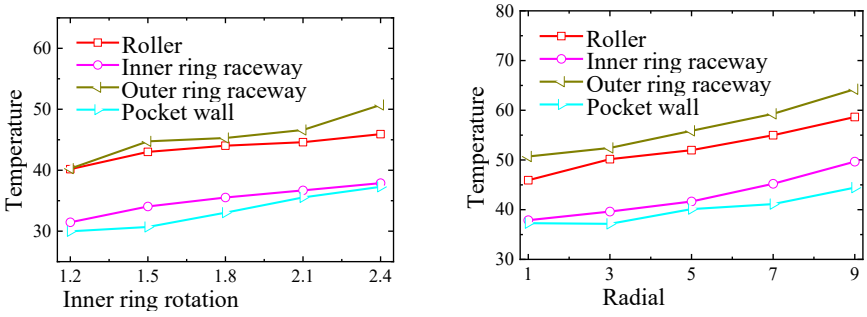

(a) at different rotation speed (b) at different radial load

Fig.8. The effect of operating conditions on the temperature of bearing components

As can be seen from Fig. 8, when the radial load is 100N, with the increase in rotation speed, the temperature of bearing each component gradually increases, the temperature of the V-shaped pocket increases from 29.9℃ to 37.2℃, and the maximum temperature difference reaches 2.5℃. When the rotation speed is 24000r/min and the radial load increases, the temperature of the V-shaped pocket increases from 37.2℃ to 44.4℃, and the maximum temperature difference reaches 2.8℃. Because the V-shaped pocket has a special pocket structure and the thermal resistance is small, it can improve the pocket's heat transfer and heat dissipation efficiency so that the pocket's temperature is relatively low.

The thermal deformation of the V-shaped pocket bearing due to temperature rise under different operating conditions is shown in Fig. 9.

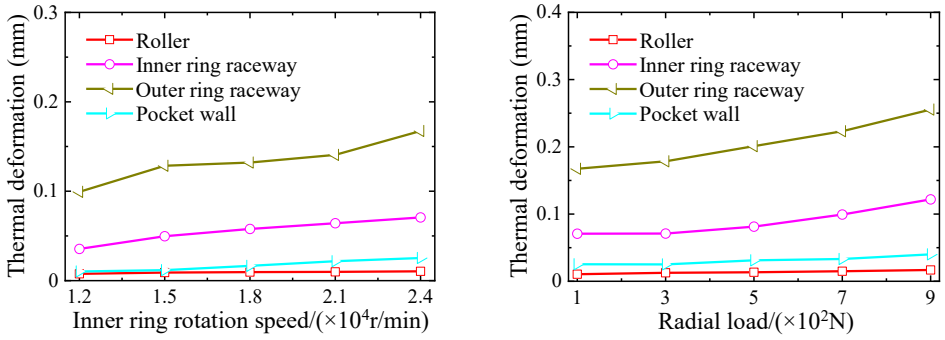

(a) at different rotation speed (b) at different radial load

Fig.9. The effect of temperature rise on thermal deformation of bearing components

Fig. 9 shows that the bearing under the influence of temperature rise, the deformation of the outer ring raceway is the most obvious, followed by the inner ring raceway, and the thermal deformation of the pocket wall is slightly higher than

the roller, it is because although the temperature of the roller is higher, its structure dimension is smaller than other parts[4].

5.3. Analysis of cage slip rate

The influence of bearing thermal deformation will inevitably lead to a change in cage stability. Therefore, the cage slip rate is utilized to judge the effect of the thermal-mechanical coupling on the V-shaped pocket bearing dynamic characteristics, and the difference in the cage stability with and without consideration of the thermal-mechanical coupling was discussed.

The change trend of the cage slip rate is shown in Fig. 10.

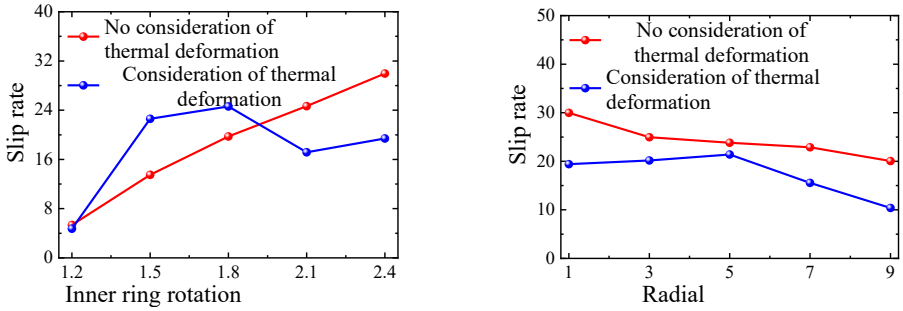

(a) at different rotation speed (b) at different radial load

Fig.10. The effect of thermal-mechanical coupling on the cage slip rate

Fig. 10(a) shows that the increase in rotation speed decreases the slip rate when the rotation speed range is 18000~21000r/min, which is different from the previous studies[24]. It is because the increase in rotation speed makes the bearing temperature rise, leading to an increase in the component deformation, reducing the relative clearance between the components, equivalent to the application of a preload on the bearing, which changes the stress state of the cage, and therefore the slip rate gradually decreases again. Fig. 10(b) shows that the slip rate gradually increases when the radial load range is 100~500N. Because the increase in load intensifies the bearing frictional heat, the component thermal deformation, and the cage instability. However, when the load is greater than 500N, under the combined action of the radial load and the centripetal force, the cage instability caused by the thermal deformation is suppressed, so the slip rate decreases with increasing load.

Comprehensively, during the bearing operation, the relative clearance between the components is reduced due to thermal deformation, which plays a certain role in reducing the cage slippage. However, this will also exacerbate bearing frictional heat generation[25], which can easily result in gluing and seizing on the contact surfaces of each component.

5.4. Analysis of contact force between roller and pocket

Under different operating conditions, Fig. 11 and 12 show the contact force variation between the roller and each V-shaped pocket wall with and without considering the influence of the thermal-mechanical coupling.

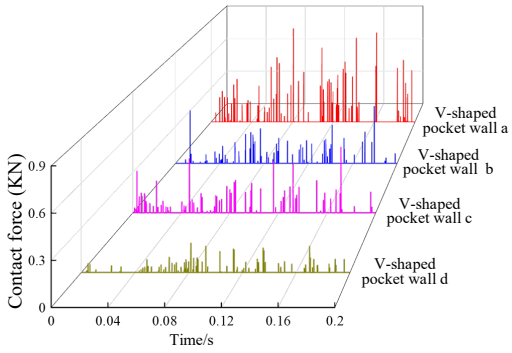

(a) rotation speed 12000r/min radial load 100N

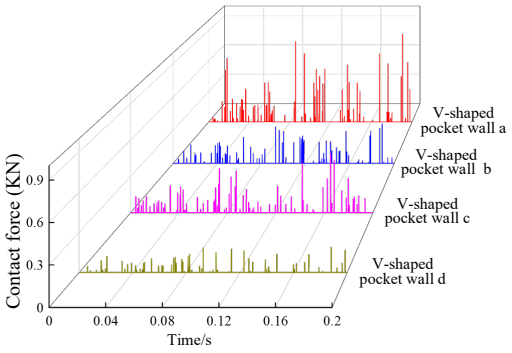

(b) rotation speed 24000r/min radial load 100N

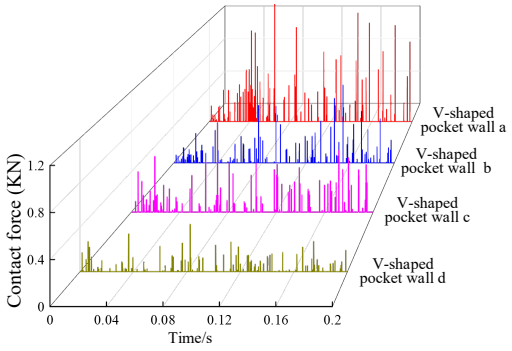

(c) rotation speed 24000r/min radial load 900N

Fig.11. Roller and pocket contact force without thermal-mechanical coupling action

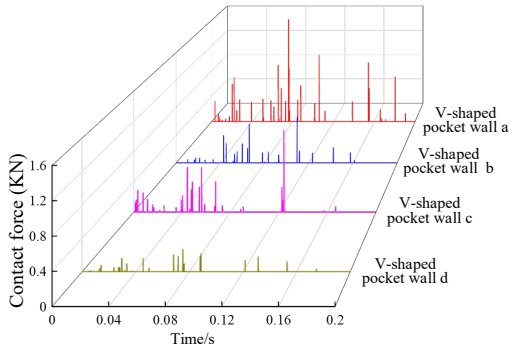

(a) rotation speed 12000r/min radial load 100N

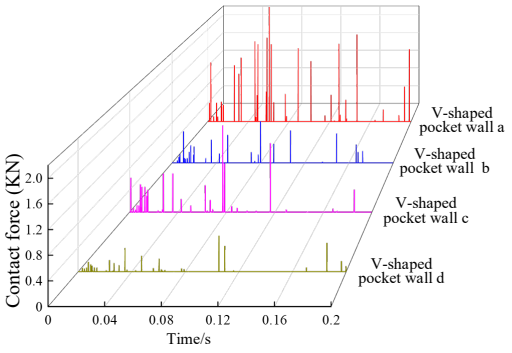

(b) rotation speed 24000r/min radial load 100N

As seen in Fig. 11 and 12, the thermal-mechanical coupling significantly affects the contact force between the roller and the pocket. Without considering the thermal-mechanical coupling, the contact force between the roller and the pocket changes slightly with the increase in rotation speed and radial load, but the collision frequency between them is higher. When the effect of the thermal-mechanical coupling is considered, the contact force between the roller and the pocket increases significantly, but the collision frequency is lower than without considering the thermal-mechanical coupling.

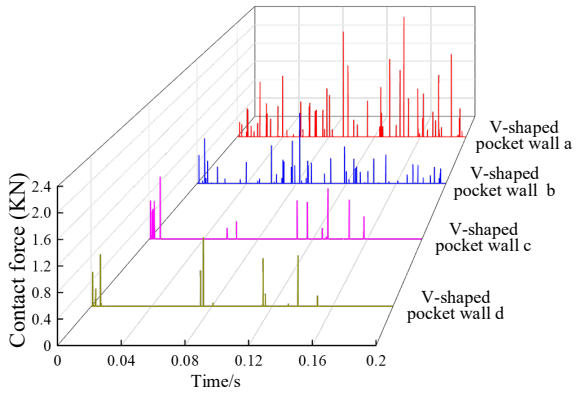

(c) rotation speed 24000r/min radial load 900N

Fig.12. Roller and pocket contact force with thermal-mechanical coupling action

In addition, the collision between the roller and the pocket mainly focuses on the wall surfaces a and b, which leads to a relatively large contact force.

6. Conclusions

In this paper, the V-shaped pocket cylindrical roller bearing has been taken as the research object, based on the multi-node thermal network model, to explore the influence of V-shaped pocket on the bearing internal heat transfer. The temperature change of the bearing each node and the thermal deformation of the components under different operating conditions were obtained, and the effects of the thermal-mechanical coupling on the bearing dynamic characteristics were analyzed. The results show that, with the increase of rotation speed and load, the increase in temperature and thermal deformation between the roller and V-shaped pocket is small. However, the deformation of the V-shaped pocket bearing caused by frictional heat significantly affects its dynamic characteristics.

Acknowledgment

The research was funded by the National Natural Science Foundation of China (Grant No.52175086).

REFERENCES

[1]. *C.L. Lei, K. Liu, R.Z. Song*, "Dynamic characteristics of angular contact ball bearings with localized defects considering thermal effect", Journal of Vibration and Shock, **vol.41**, no.18, 2022, pp.33-40.

[2]. *X. Hao*, Research on thermal characteristics of cylindrical roller bearing and its effect on vibration response of rotor system, P.D. Thesis, Dalian University of Technology, 2020.

[3]. *K. Yan, J. Hong, J. Zhang*, *J.H. Zhang, W. Mi, W.W. Wu*, "Thermal-deformation coupling in thermal network for transient analysis of spindle-bearing system", International Journal of Thermal Sciences, no.104, 2016, pp.1-12.

[4]. *J. Yu, S.Y. Li, W. Yuan*, *X.Y. Chen*, "Dynamic property of spindle bearing considering the effect of thermal deformation", Journal of Aerospace Power, **vol.33**, no.2, 2018, pp.477-486.

[5]. *S.S. Cao, H.S. Yang, B. Luo*, *R. Tang, S.E. Deng*, "Dynamic analysis of aero-engine spindle ball bearings with thermal-mechanical coupling", Journal of Aerospace Power:1-14[2023-07-13].DOI:10.13224/j.cnki.jasp.20220890.
[6]. *W.J. Gao, Z.X. Liu, P.F. Zhu*, *Y.G. Lv*, "Steady thermal analysis of main-shaft roller bearing for aero-engine based on multi-nodes thermal network methods", Journal of Propulsion Technology, **vol.40**, no.2, 2019, pp.382-388.
[7]. *C. Zhang, J.Y. Tian, D. Guo*, *Q.B. Niu*, "Thermal characteristics of grease lubricated high-speed angular contact ball bearings with thermal deformation", Journal of Tsinghua University(Science and Technology), **vol.62**, no.3, 2022, pp.482-492.
[8]. *Y.B. Liu, Z.H. Deng and D.Y. Sang*, "High-speed dynamic performance of cylindrical roller bearing with V-shape pocket", Acta Aeronautica et Astronautica Sinica, **vol.42**, no.7, 2021, pp.579-590.
[9]. *A. Harrist, M.N. Kotzalas*, Advanced concepts of bearing technology: rolling bearing analysis, Fifth edition. New York: CRC Press, Taylor& Francis Group. 2006.
[10]. *Y.T. Fei, G.H. Li, R.S. Lu*, Theory and application of mechanical thermal deformation. Beijing: Arms industry Press, 2009, pp.153-157.
[11]. *Y.X. Chen*, Research on vibrations of cylindrical roller bearings based on contact mechanics, P.D. Thesis, Huazhong University of Science & Technology, 2005.
[12]. *A. Palmgren*, Ball and roller bearing engineering. Philadelphia, USA: SKF Industries Inc., 1959.
[13]. *D. Dowson, G.R. Higginson*, Elastohydrodynamic lubrication. London: Pergamon Press, 1977.
[14]. *T.L.H. Walford, B.J. Stone*, "The sources of damping in rolling element bearings under oscillating conditions", Proceedings of the Institution of Mechanical Engineers, Part C: Journal of Mechanical Engineering Science, **vol.197**, no.4, 1983, pp.225-232.
[15]. *D. Dowson, G.R. Higginson*, "A numerical solution to the elasto-hydrodynamic problem", Journal of mechanical engineering science, **vol.1**, no.1, 1959, pp.6-15.
[16]. *D.Y. Sang*, *Y.B. Liu*, *X.Z. Sun and Z.H. Deng*, "Wear performance of geometric parameters of V-shape pocket of cylindrical roller bearing", Journal of Aerospace Power, **vol.38**, no.2, 2023, pp.473-481.
[17]. *W.H. Qian*, Dynamic simulation of cylindrical roller bearings, P.D. Thesis, Aachen, Germany: RWTH Aachen University, 2014.
[18]. *J. Huang, Y.B. Liu, X.Y. Li*, "Analysis of high speed thermal characteristics of V-shaped pocket cylindrical roller bearing", UPB Scientific Bulletin, Series D: Mechanical Engineering, **vol.85,** no.3, 2023, pp.145-166.
[19]. *J.A. Henao-Sepulveda, M. Toledo-Quinones, Y. Jia*, "Contactless monitoring of ball bearing temperature", IEEE, Instrumentation and Measurement Technology Conference Proceedings, 2005, pp.1571-1573.
[20]. *D.X. Zheng, W.F. Chen*, "Effect of structure and assembly constraints on temperature of high-speed angular contact ball bearings with thermal network method", Mechanical Systems and Signal Processing, **vol.145**, 2020, pp.106929.
[21]. *C. Su, W.F. Chen*, "An improved model of motorized spindle for forecasting temperature rise based on thermal network method", The International Journal of Advanced Manufacturing Technology, **vol.119**, no.9-10, 2022, pp.5969-5991.
[22]. *R.A. Burton, H.E. Staph*, "Thermally activated seizure of angular contact bearings", ASLE Transactions,**vol.10**, no.4, 1967, pp.408-417.
[23]. *R. Kerrouche, A. Dadouche, M. mamou*, *S. Boukraa*, "Power loss estimation and thermal analysis of an aero-engine cylindrical roller bearing", Tribology Transactions, **vol.64**, no.6, 2021, pp.1079-1094.
[24]. *Q.Q. Yuan, Y.S. Zhu, J.H. Zhang*, *M.Y. Yang, K. Yan, J.* Hong, "Cage dynamic characteristic of precision rolling ball bearings considering lubrication collision", Journal of Xi'an Jiao tong University, **vol.55**, no.1, 2021, pp.110-117.
[25]. *K. Yan, Y.T. Wang, Y.S. Zhu, J. Hong, Q. Zhai*, "Investigation on heat dissipation characteristic of ball bearing cage and inside cavity at ultra high rotation speed", Tribology International, no.93, 2016, pp.470-481.